Advances in GPR data acquisition and analysis for archaeology

Wenke Zhao,[1,2,3] Gang Tian,[2,4] Emanuele Forte,[1] Michele Pipan,[1] Yimin Wang,[2] Xuejing Li,[2] Zhanjie Shi[4] and Haiyan Liu[2]

[1]*Department of Mathematics and Geosciences, University of Trieste, I-*34127 *Trieste, Italy. E-mail: zwenk@163.com*
[2]*Department of Earth Sciences, Zhejiang University,* 310000 *Hangzhou, China*
[3]*The International Centre for Theoretical Physics (ICTP), I-*34151 *Trieste, Italy*
[4]*Academy of Cultural Heritage, Zhejiang University,* 310000 *Hangzhou, China*

Accepted 2015 March 10

SUMMARY

The primary objective of this study is to evaluate the applicability and the effectiveness of ground-penetrating radar (GPR) to identify a thin burnt soil layer, buried more than 2 m below the topographic surface at the Liangzhu Site, in Southeastern China. The site was chosen for its relatively challenging conditions of GPR techniques due to electrical conductivity and to the presence of peach tree roots that produced scattering. We completed the data acquisition by using 100 and 200 MHz antennas in TE and TM broadside and cross-polarized configurations. In the data processing and interpretation phase, we used GPR attribute analysis, including instantaneous phase and geometrical attributes. Validation analysis ground-truthing performed after the geophysical surveys, validated the GPR imaging, confirmed the electrical conductivity and relative dielectric permittivity (RDP) measurements performed at different depths, and allowed a reliable quantitative correlation between GPR results and subsurface physical properties. The research demonstrates that multiple antenna configurations in GPR data acquisition combined with attribute analysis can enhance the ability to characterize prehistoric archaeological remains even in complex subsurface conditions.

Key words: Image processing; Electrical properties; Electromagnetic theory; Ground penetrating radar; Magnetic and electrical properties.

INTRODUCTION

The ground-penetrating radar (GPR) is a non-invasive geophysical method that can accurately map the spatial extent of near-surface objects and archaeological features via the propagation and reflection at impedance boundaries of an electromagnetic wave generated by a transmitter deployed at the surface or, less commonly, within a borehole (Slob *et al.* 2010; Everett 2013). The GPR resolution capability, also depending on antenna frequency and soil properties, by far greater than that obtained by other geophysical methods, makes this technique suitable for high-resolution shallow studies. Since numerous commercial instruments were developed during 1970s and 1980s (Morey 1974; Davis *et al.* 1985), GPR has come into a well-accepted technique in archaeology (e.g. Bevan & Kenyon 1975; Batey 1987; Conyers & Goodman 1997; Clarke *et al.* 1999; Pipan *et al.* 2001; Leckebusch 2003; Vafidis *et al.* 2005; Forte & Pipan 2008; Booth *et al.* 2010; Conyers 2010, 2011; Viberg *et al.* 2011; Goodman & Piro 2013).

The primary goal of most GPR surveys in archaeology is to identify and define the size, shape, depth and location of buried cultural remains and related stratigraphy (Conyers 2012). The most straightforward way to accomplish this task is by identifying and correlating important reflections within 2-D profiles, at depths from a few tens of centimetres to 5 m (Davis & Annan 1989; Fisher *et al.* 1992). Furthermore, archaeological geophysicists have appreciated that a better understanding of the spatial extent of targets is obtained from a grid, rather than a profile, of GPR data (e.g. Goodman *et al.* 1995; Neubauer *et al.* 2002; Gaffney *et al.* 2004). The use of 3-D GPR (in real words 'pseudo 3-D' GPR, that is the combination of several 2-D profiles) is steadily increasing in archeological surveys throughout the world (e.g. Nuzzo *et al.* 2002; Leucci & Negri 2006; Booth *et al.* 2008; Gaffney 2008; Yalçiner *et al.* 2009; Bini *et al.* 2010; Drahor *et al.* 2011). True 3-D multichannel GPR arrays were also introduced recently, which allow development of increasingly sophisticated acquisition and processing techniques and further resolution enhancement (Francese *et al.* 2009; Linford *et al.* 2010; Trinks *et al.* 2010; Lualdi & Lombardi 2014). However, common offset measurements are nonetheless quicker to perform and to process and are still the most popular data acquisition method (Conyers 2013; Trinks *et al.* 2014; Urban *et al.* 2014).

The basics of GPR data acquisition, processing and interpretation are now commonplace to most archaeological geophysical practitioners (Conyers & Leckebusch 2010). While it is important and appropriate to continue working at sites with traditional acquisition and processing methods to prospect for buried archaeological remains, we propose that there are still many advances

of this technique that can be followed as that, to test ideas about buried archaeological remains in ways not possible using traditional GPR acquisition methods, and to take new processing and interpretation methods that can produce greater precision in the products produced, while revealing more information about buried archaeological features.

The search and characterization of earthen archaeological features is an important topic in geophysical prospecting for archaeology due to the large temporal and spatial distribution of such type of cultural heritage. Earthen archaeological features include rammed platforms, earth ovens, ancient earth walls, kiln sites, storage pits and tumuli, mostly related to prehistoric settlements. From the point of view of geophysical prospecting, the characterization of earthen archaeological features are challenging because of the limited target/background contrast (Conyers 2004; Weaver 2006; Forte & Pipan 2008) and the attenuation of the electromagnetic waves caused by the relatively high electrical conductivity of clay-rich soils, which are frequently used as building materials due to their mechanical properties. Therefore, it is important to develop new techniques to enhance imaging and characterization of such prehistoric/historic sites, in order to identify and map archaeological remains and optimize archaeological excavation plans.

We propose a method based on three GPR antenna configurations in data acquisition to obtain improved radar images, considering that the polarization of the signal measured by the receiving antenna is a function of the orientation of radar antennas with respect to the unknown orientation of potential targets. GPR polarization is an important issue when designing a GPR survey and is useful to constrain the size, shape, orientation and electrical properties of buried objects (Roberts & Daniels 1996; Radzevicius & Daniels 2000). The polarization properties of GPR waves have been widely analyzed for geological and engineering applications (Pipan *et al.* 2000; Radzevicius & Daniels 2000; Tsoflias *et al.* 2004; Capizzi & Cosentino 2008; Sassen & Everett 2009), but have found limited exploitation in archaeological prospecting to date.

In the processing and interpretation phase, we add GPR attribute analysis into the standard sequence, including different combinations of physical and geometrical attributes, to produce improved images of otherwise invisible features. Attribute analysis is increasingly used in GPR data interpretation (Grasmueck 1996; Forte *et al.* 2012), and has been successfully applied in GPR archaeological prospection (Böniger & Tronicke 2010; Creasman *et al.* 2010; Zhao *et al.* 2013a,b, 2015).

We tested the proposed procedure in the GPR study at the Liangzhu Site, a famous Neolithic culture centre in Southeastern China. The main objective was to evaluate the applicability and the effectiveness of the method to identify a thin burnt soil layer, buried more than 2 m below the surface. The burning process produced an increase in soil susceptibility, an effect that has been extensively exploited in archaeological prospecting by applying magnetic methods to identify targets with thermoremanent magnetization (e.g. Tite & Mullins 1971; Oldfield & Crowther 2007; Kostadinova-Avramova & Kovacheva 2013). However, a preliminary magnetic study demonstrated that the magnetic contrast is weak and discontinuous in the study area, possibly due to the low magnetization and to the burial depth.

The presence of a large number of peach trees in the study area adds a further element of complexity to the GPR study, because of the scattering produced by the roots. Two cores with measurements of relative dielectric permittivity (RDP) and electrical conductivity at different depths allowed calibration and validation of the GPR results on a constrained physical basis.

Study area and previous geophysical work

The Liangzhu site, located at the lower reaches of Qiantang River (Fig. 1), is a famous Neolithic jade culture centre in Southeastern China. Historically it was part of an ocean bay, which gradually piled up towards a vast expanse of fertile plain. This place represents one of the earliest Chinese settlements, where the Liangzhu Culture flourished, the richest and most vivid civilization in China.

The Liangzhu Culture developed about 5400–4300 yr ago, but suddenly disappeared from the Taihu Lake area about 4200 yr ago when it reached the peak. In 1930s the archaeologists discovered the first evidences of prehistoric culture and many jade,

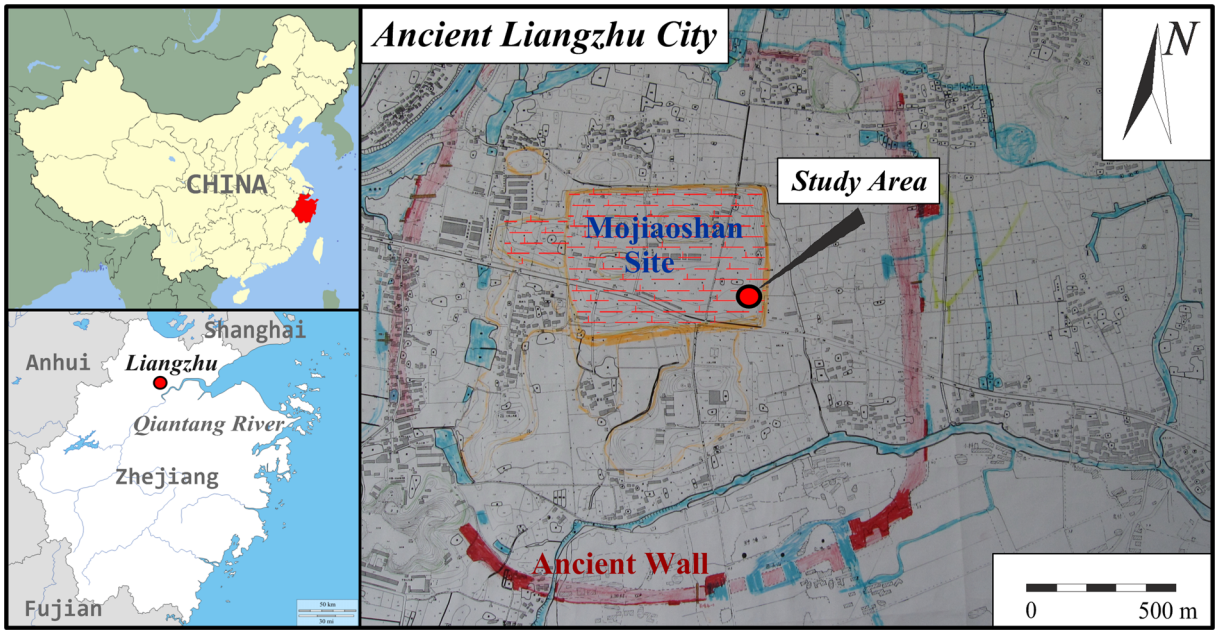

Figure 1. Location map of the Liangzhu Site, Zhejiang, Southeastern China.

silk, ivory and pottery objects at Liangzhu, Zhejiang Province. The first archaeological excavation was performed by Xingeng Shi in 1936 (Shi 1938). The successive excavations proved that such culture had advanced handicraft and agricultural skills, including jade and pottery processing, irrigation, paddy rice cultivation and aquaculture. Moreover, rammed earth remains of the ancient city wall, 40 to 60 m wide, were discovered at the Liangzhu site in 2007 (Liu 2008). The total area of the ancient city was 2 900 000 m^2, and the site was considered as the centre of the Liangzhu culture.

The study area is located at the southeastern side of Mojiaoshan Site in the centre of the ancient city, an artificial rammed earth platform, which has been recognized as possible remains of prehistoric buildings (Zhao 2001). The dimensions of such platform are about 670 and 450 m in E–W and N–S direction, respectively. It is partially covered by cultural layers of different periods, mainly including modern agricultural soil and sandy soil of the Han Dynasty (about 2000 yr ago). A peach orchard presently covers the area. The thickness of the Neolithic rammed earth layer is about 10 m and a burnt soil layer, with mixed ash and charcoal powder, has just been found in the southeastern portion of the platform, buried more than 2 m below the surface. The possible origin of the layer could be an ancient fire disaster or worship activities, but it is not clear yet.

Previous GPR studies provided a limited amount of useful information about the buried prehistoric cultural heritage of the Liangzhu Site, due to the effect of water saturated clay-rich soils. For example, experiments performed with different antennas, including 1 GHz and 500 MHz with a trace distance 0.01 m, and 250, 200 and 100 MHz with a trace distance 0.05 m, hardly imaged a 1 m deep layer of stones, with average diametre larger than 20 cm.

We focused on the rammed earth platform and applied polarization data acquisition and attribute based data processing techniques to evaluate the applicability of non-conventional GPR methods to the study of prehistoric archaeological targets in challenging subsurface conditions.

Data acquisition and processing

We performed data acquisition with a PulseEKKO PRO System (Sensors and Software Inc.), equipped with 100 and 200 MHz unshielded antenna pairs (Fig. 2a). We manually triggered the GPR

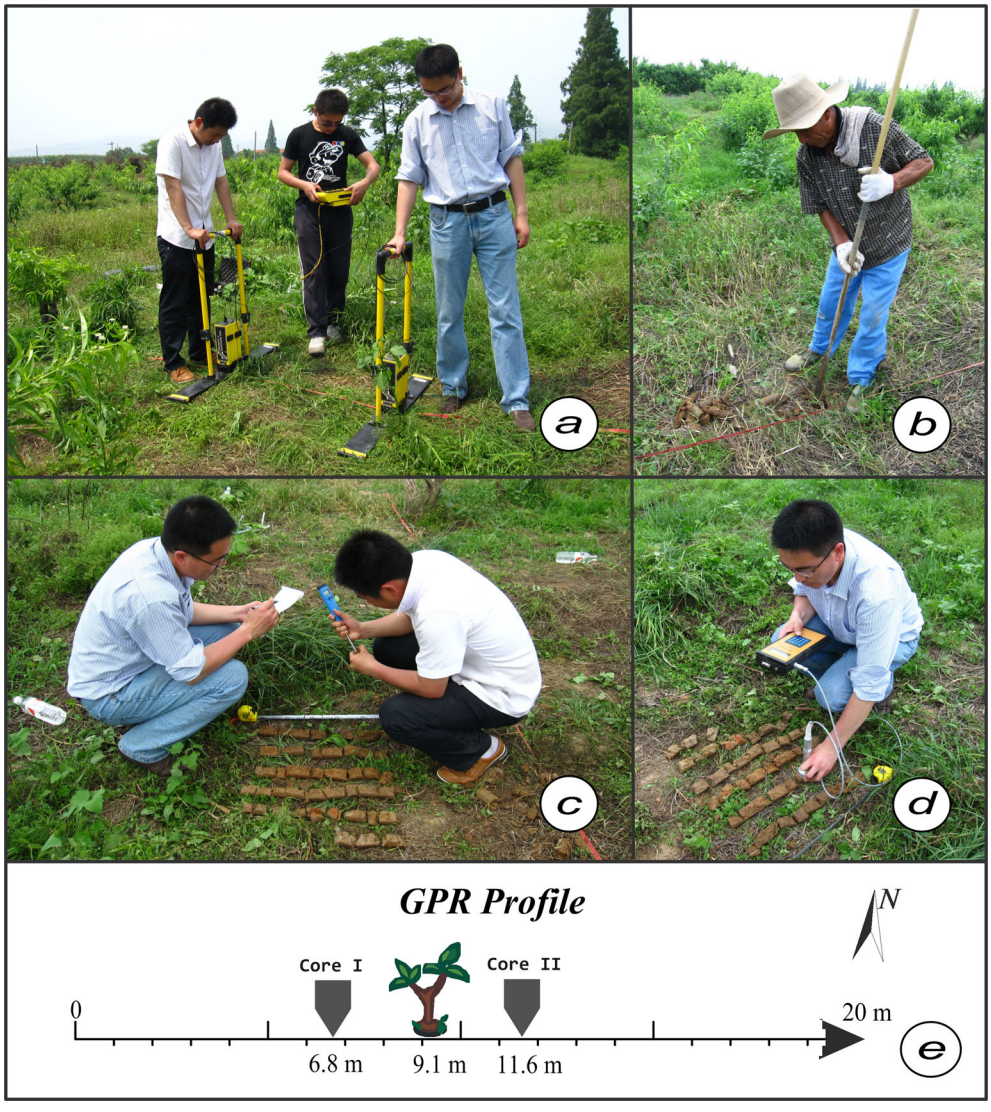

Figure 2. Photographs showing different data acquisition on the archaeological field. (a) GPR survey with 100 MHz antennas; (b) drilling cores with *Luoyang Spade*; (c) electrical conductivity measurement; (d) RDP measurement; (e) sketch of the GPR data acquisition.

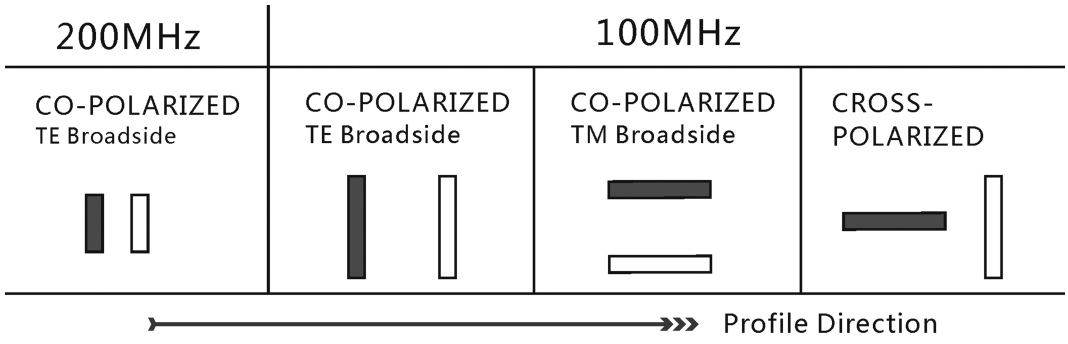

Figure 3. Antenna configurations used in the GPR study. Grey and white blocks represent the transmitting and receiving antennas, respectively. The offsets of 200 and 100 MHz antennas are 0.5 and 1 m, respectively.

at a constant spacing of 0.1 m to ensure an accurate positioning. The total length of the survey line was 20 m. Un-desired effects from tree roots were expected at 9.1 m from the beginning of the GPR profile, the location of a small peach tree. We applied three antenna configurations to exploit the polarization effects due to the orientation of antennas, targets and tree roots (Fig. 3).

Following the GPR survey, we performed two cores at 6.8 and 11.6 m with a *Luoyang Spade* (the most popular drilling tool in Chinese archaeological field operations), to calibrate and validate the GPR results. We did not only identify and classify the types of soils in the cores with the help of archaeologists, but also measured the electrical conductivity and RDP at different depths with two portable instruments: HI 98311 waterproof EC/TDS metre, produced by Hanna Instruments Inc., and Percometer v.7, manufactured in Estonia by Adek Ltd., respectively (Figs 2c and d).

We applied the following processing flow on all the common offset GPR profiles recorded:

(1) data editing;
(2) dewow;
(3) amplitude analysis;
(4) design and application of a bandpass *filtering* (corner frequencies: 20–40–220–260 and 40–60–300–340 MHz on 100 and 200 MHz radar data, respectively);
(5) SEC (spreading & exponential compensation) gain;
(6) velocity analysis;
(7) attribute analysis.

The radar-wave velocity was calculated from wide offset CMPs at selected positions. The estimated velocities range between 6.0 and 10.0 cm ns^{-1} according to velocity spectra and direct analysis of reflections in CMP gathers (Fig. 4). We integrated such data with diffraction hyperbola analysis performed on common offset sections, and eventually calculated a mean 7.5 cm ns^{-1} EM wave velocity.

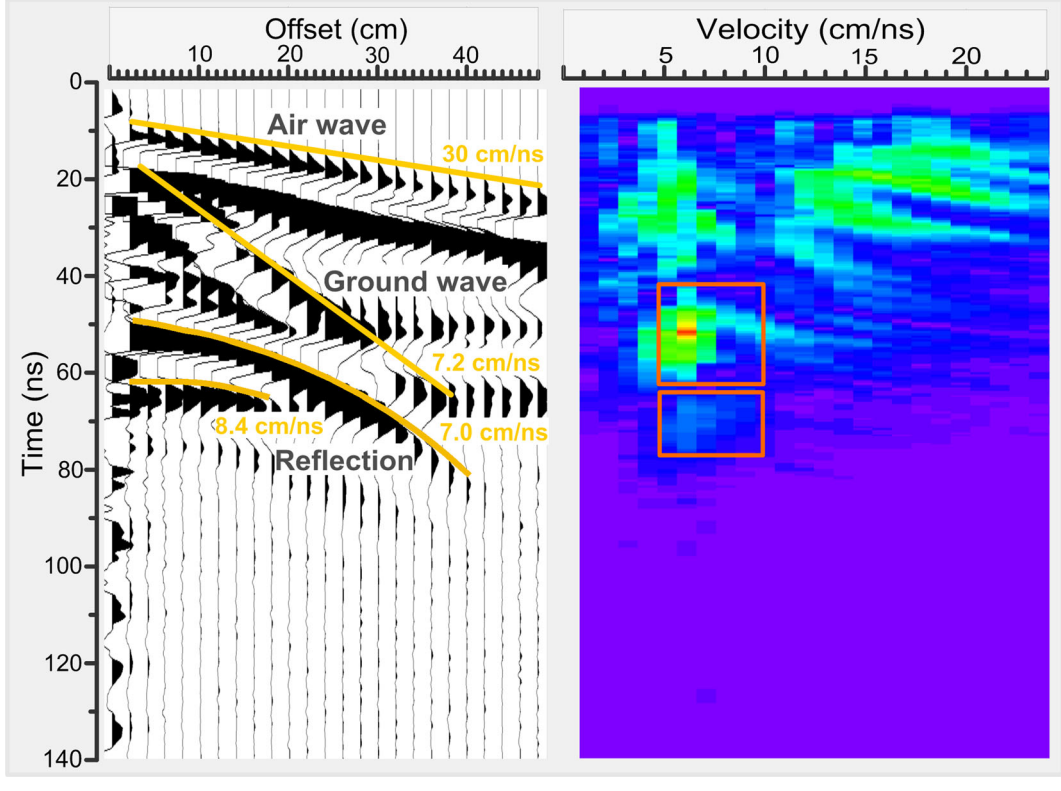

Figure 4. Velocity analysis performed on a CMP and the corresponding velocity spectrum (semblance velocity panel).

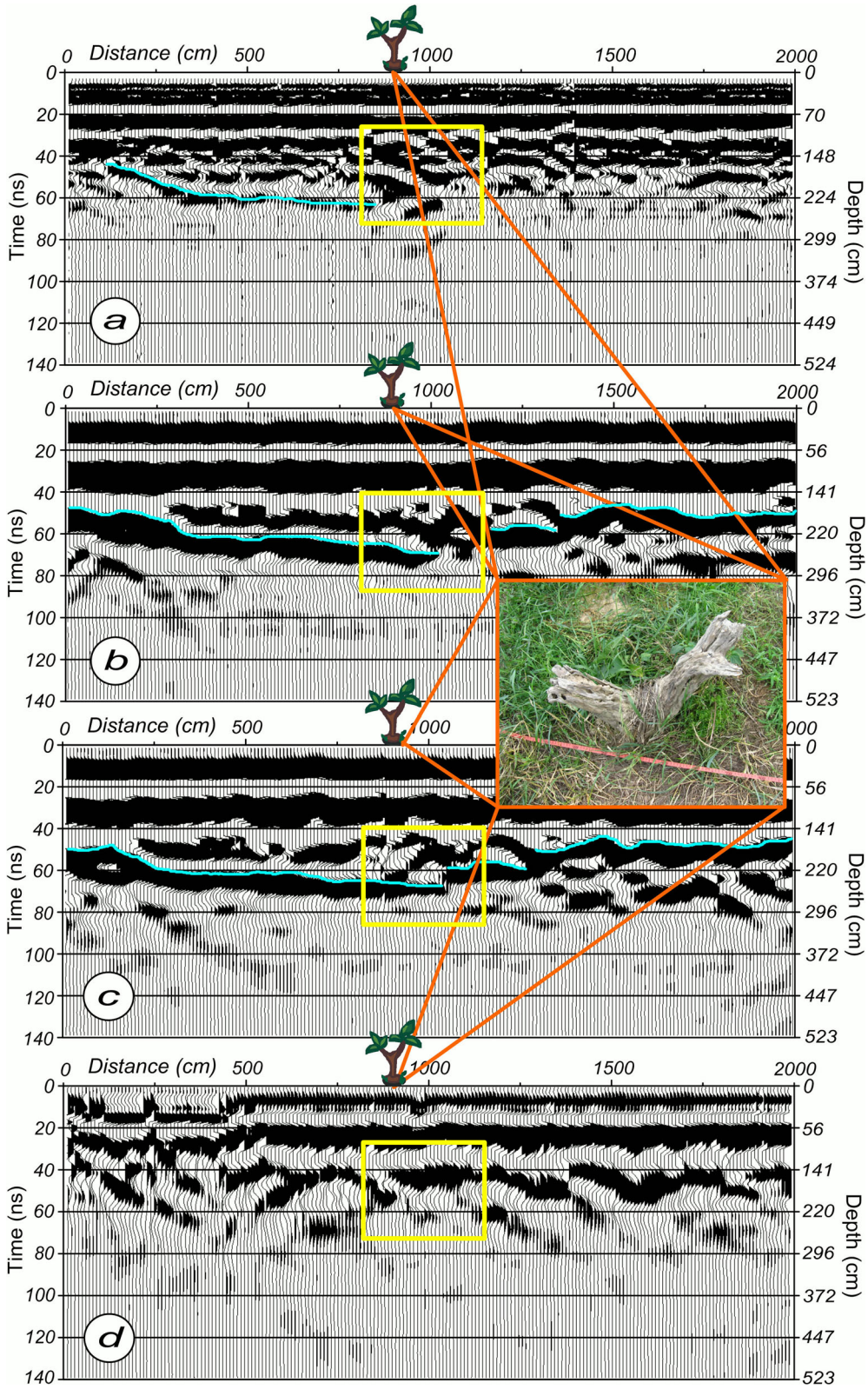

Figure 5. 2-D GPR amplitude profiles. (a) 200 MHz antennas in TE broadside configuration; (b) 100 MHz antennas in TE broadside configuration; (c) 100 MHz antennas in TM broadside configuration; (d) 100 MHz antennas in cross-polarized configuration. Light blue lines indicate the continuous reflection related with the potential archaeological target, while the yellow rectangle indicates a scattering zone interpreted as the interference effect due to the peach tree roots.

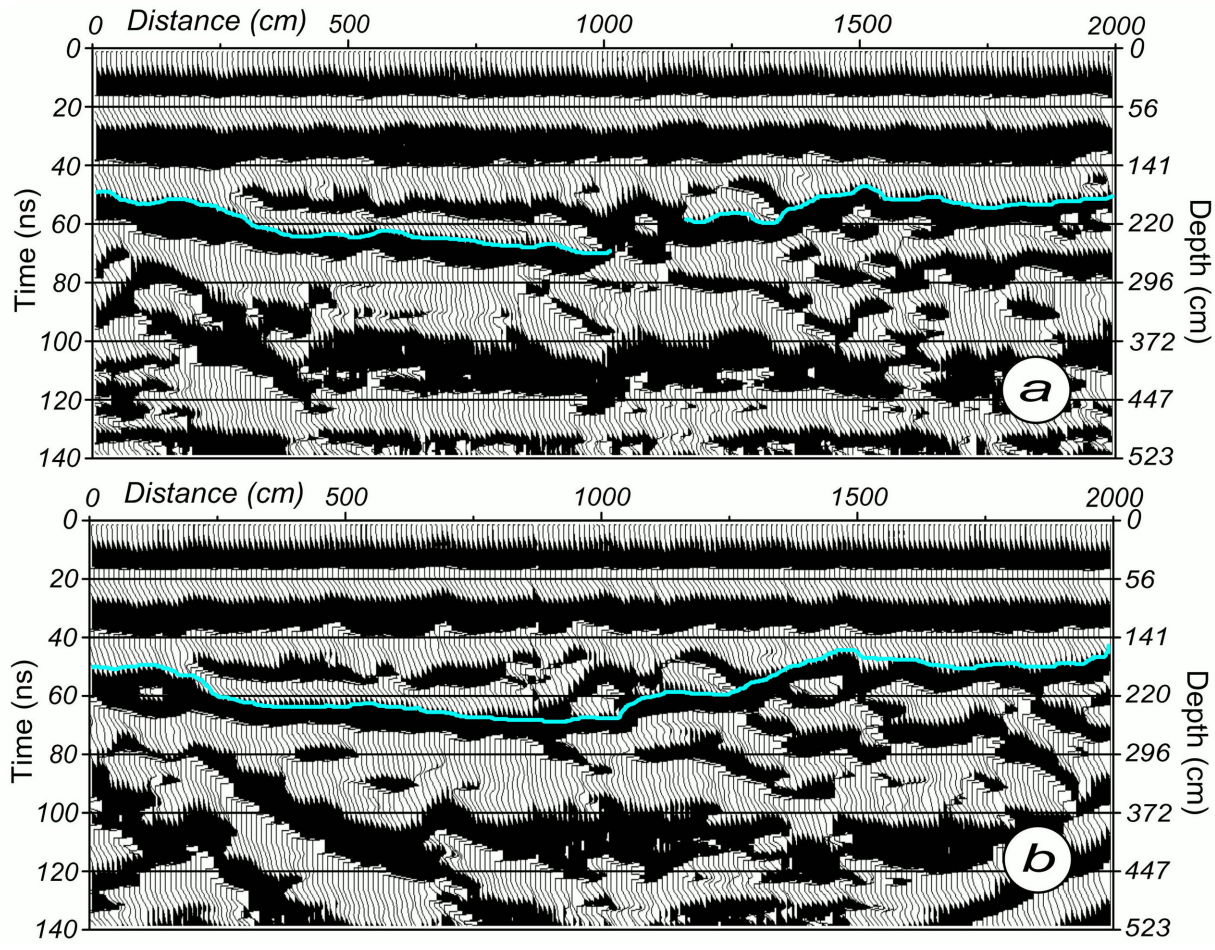

Figure 6. 2-D GPR instantaneous phase profiles. (a) 100 MHz antennas in TE broadside configuration; (b) 100 MHz antennas in TM broadside configuration. Light blue lines indicate the continuous reflection related to the potential archaeological targets.

The time-to-depth conversion was based on:

$$d = \frac{1}{2}\sqrt{(vt)^2 - x^2},$$

where d is depth of the target, v is radar-wave velocity, t is travel time and x is the offset.

As for target identification and characterization, we performed the analysis of instantaneous phase and local standard deviation. Instantaneous phase emphasizes spatial continuity/discontinuity of reflections by providing a way for weak and strong events to appear with equal strength, since it is independent from the amplitude. On the other hand, local standard deviation, as a typical geometrical attribute, is generally utilized in seismic stratigraphic interpretation (Taner *et al.* 1994). In order to focus on the visibility of the continuity characteristics of GPR data, such geometrical attribute was calculated on the instantaneous phase profile. The proposed strategy could improve the recognition of the burnt soil layer obviously.

RESULTS

The TE-broadside is the most widely used GPR configuration (e.g. Reynolds 2011; Everett 2013) and we used it to perform a preliminary comparison test between 200 and 100 MHz antennas. In Figs 5(a) and (b), a high-reflective layer (light blue) with good lateral continuity is apparent between 0 and 9 m and the depth of such layer reaches a maximum of 68 ns (approximately 250 cm depth, by taking into account the offset and the estimated average 7.5 cm ns^{-1} velocity). The reflection terminates between 9 and 10 m, in a chaotic zone interpreted as the interference due to peach tree roots. The lower central frequency (i.e. 100 MHz, Fig. 5b) allows better identification of reflectors in the deeper part of the section, at the expected burial depth of the archaeological remains in the area (not less than 2 m, that is at two-way times larger than 50 ns). In addition, the difference of the reflective characteristics between the two GPR profiles is apparent in the segment between 10 m and the end of the section, because of different subsurface conditions, such as moisture variations of the sediments.

The TM broadside configuration shows better performances in imaging and discrimination of targets at the depth of archaeological interest, by weakening the interference caused by the tree roots (see Fig. 5c), as the polarization effects are a function of the relative orientation of radar antennas and the potential targets. We therefore tested it to improve the overall signal-to-noise ratio and the identification performance in the depth range of archaeological interest. It is difficult to identify any reflection from potential archaeological targets in the cross-polarized profile, while the effect related to the tree roots is clearer (Fig. 5d).

We calculated the instantaneous phase of the data obtained with different configurations to focus on the burnt layer and enhance the performance in target detection. Fig. 6 shows that such attribute allows identification of the reflector with high continuity

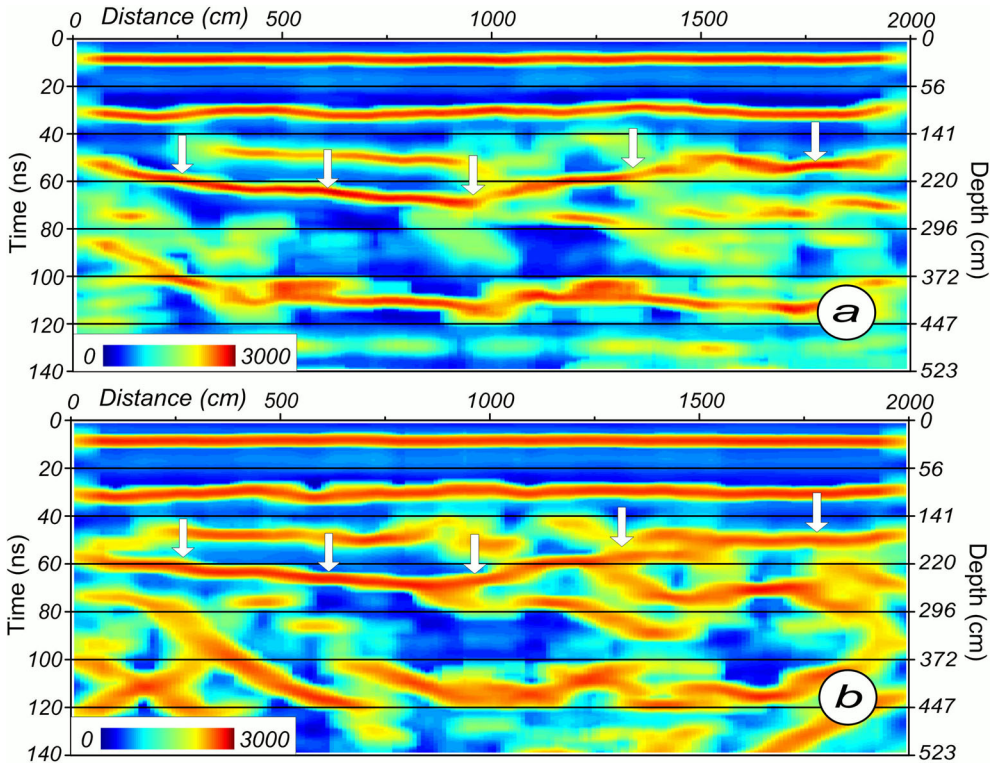

Figure 7. 2-D GPR geometrical attribute, calculated on the instantaneous phase. (a) 100 MHz antennas in TE broadside configuration; (b) 100 MHz antennas in TM broadside configuration.

along the whole section. Furthermore, we used the local standard deviation, based on the instantaneous phase attribute, to make the interpretation easier and more constrained (Fig. 7). Such geometrical attribute can improve the interpretation by emphasizing the continuity/discontinuity properties and by enhancing the attainable resolution. Chaotic zones are identified by the lowest lateral coherencies, while homogeneous materials show higher lateral coherencies. Fig. 7 shows that the geometrical attribute analysis allows higher precision in both target detection and location, supplying more details about the target morphology. Moreover, such attribute can minimize the scattering/interference effects, performing very well even where the signal-to-noise ratio is lower. The analysis of the interpretation results obtained from the application of local standard deviation analysis on different co-polarized antenna configurations shows a perfect match and indicates that the attribute is robust and not sensitive to noise and interferences, such as those produced by the peach tree root.

Fig. 8 shows the cores: different cultural layers sequentially buried beneath the surface were identified and described by the archaeologists. The burnt soils are mixed with ash and charcoal powder, and they are buried at 2.5 and 2.2 m depth at Core I and Core II, respectively. According to the sequence of the soil layers, the depositions can be classified schematically as follows:

(1) Layer ‘a’, modern grey agricultural soil;
(2) Layer ‘b’, grey sandy soil of the Han Dynasty (about 2000 yr ago);
(3) Layer ‘c’, Neolithic brown rammed earth above the burnt soil;
(4) Layer ‘d’, Neolithic burnt soil;
(5) Layer ‘e’, Neolithic brown rammed earth below the burnt soil.

We measured the electrical conductivity and RDP of the core samples in the field soon after the drilling, to limit variations of moisture content and to ensure the reliability of the measured physical parameters. The average of three measurements was taken as representative value of each depth interval. Tables 1 and 2 present the soil sample values measured at Core I and Core II, respectively. The electrical conductivity (DC value) of the burnt soil is different from the surrounding soils, but the most significant feature is that the RDP of the burnt soil differs greatly from the surrounding rammed earth, which is the physical basis, producing the distinct reflections, observed in the GPR sections.

DISCUSSIONS AND CONCLUSIONS

A combination of different antenna configurations and attributes of the radar trace is an effective strategy to detect low contrast archaeological targets in noisy environments. The proposed procedure was successfully tested to identify a burnt soil layer, characterized by limited thickness low target/background contrast at a representative prehistoric archaeological site. Low central-frequency antennas (i.e. 100 MHz) give clear evidence of continuous buried remains. Combined with limited validation analysis ground-truthing, the GPR interpretation extends the localized borehole information about the depth of the burnt layer and provides clear information about its morphology and lateral continuity (Fig. 9).

The electrical conductivity measurements indicate increasing values from Core I to Core II. Thus, the relatively high conductivity is the likely responsible for the attenuation observed in the 200 MHz data. In addition, two further boundaries between different cultural layers above the main target are poorly imaged by the GPR profiles, which may be related to the RDP values of the materials: there is actually no significant differences between Layers ‘a’ and ‘b’, and

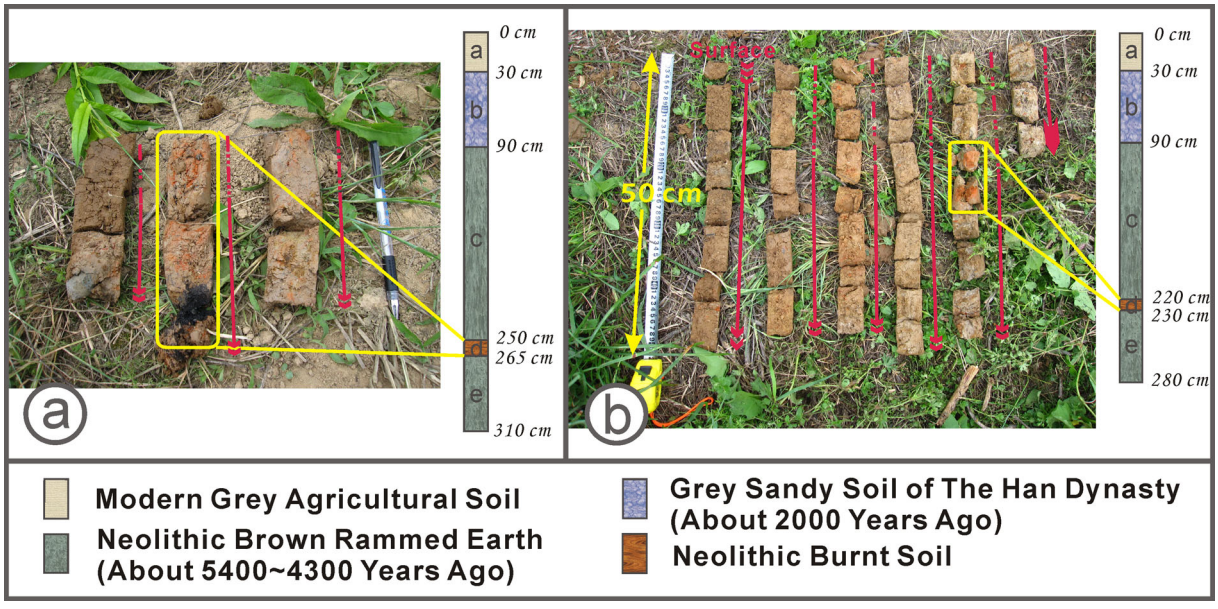

Figure 8. Archaeological interpretation based on cores. (a) Core I; (b) Core II.

Table 1. Electromagnetic parameters measured on the Core I samples. The burnt level is highlighted in grey.

Layer	Depth (cm)	σ (mS cm^{-1})	RDP
a	0–30	0.12 ± 0.05	20 ± 1
b	30–90	0.06 ± 0.05	18 ± 1
c	90–180	0.12 ± 0.05	20 ± 1
	180–220	0.16 ± 0.05	21 ± 1
	220–250	0.18 ± 0.05	21 ± 1
d	250–265	0.12 ± 0.05	14 ± 1
e	265–280	0.20 ± 0.05	19 ± 1
	280–310	0.28 ± 0.05	20 ± 1

Table 2. Electromagnetic parameters measured on the Core II samples. The burnt level is highlighted in grey.

Layer	Depth (cm)	σ (mS cm^{-1})	RDP
a	0–30	0.05 ± 0.05	18 ± 1
b	30–90	0.08 ± 0.05	20 ± 1
c	90–180	0.16 ± 0.05	21 ± 1
	180–220	0.35 ± 0.05	20 ± 1
d	220–230	0.19 ± 0.05	15 ± 1
e	230–280	0.4 ± 0.05	19 ± 1

between Layers 'b' and 'c'. The EM impedance contrast is therefore too low to provide detectable signals. However, we also have to face the fact that the ringing TX–RX cross-talk footprint from low frequency unshielded antennas is huge compared to 900 or 500 MHz antennas, and the antenna 'ringing' has not been removed by background subtraction filter, because this would obviously remove our main detection target, the horizontal ~2.0 m deep stratigraphic layer as well. Nonetheless, 100 MHz is the optimal frequency at the test-site, considering the depth and the resolution of the burnt layer. The selection of antennas with the correct operating frequency necessary for the depth and the resolution of the features of archaeological interests is one of the most important decisions in GPR archaeological survey (Jol 1995; Smith & Jol 1995; Grealy 2006).

Nonetheless, the results obtained at the test-site with the proposed procedure provide a remarkable amount of new subsurface information compared to previous GPR experiments in the area. The present work demonstrates that a proper combination of data acquisition and processing/analysis techniques can overcome the limits of standard GPR techniques and successfully image low-contrast cultural targets such as contacts between clayey soils and rammed sandy

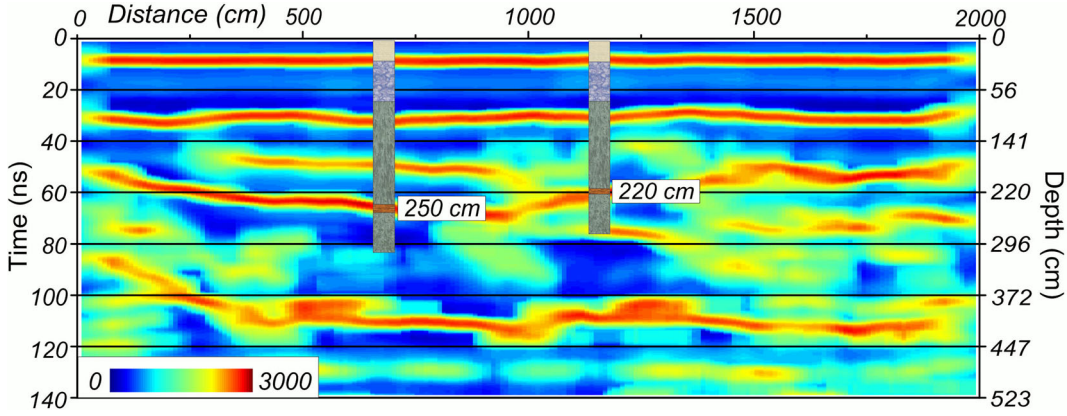

Figure 9. GPR interpretation of the section reported in Fig. 7(a), correlated with validation analysis ground-truthing.

soils, which are subsurface conditions frequently met at prehistoric sites.

In particular, polarization effects can be exploited in the data acquisition phase to minimize the interferences from linear objects, such as pipes, wires, rebars or roots in the near subsurface. A great deal of work is nonetheless required to design optimal surveys and to extract the desired information by the fact that dimensions and orientation of linear objects that can produce interferences are often unknown.

The applications of GPR attribute analysis indicate that both detectability and resolution can be enhanced within the physical limits of the methods and improved subsurface images can be produced. By using GPR attributes we demonstrate that it is possible to attain higher levels of confidence in identification and characterization of culture heritage, even using just one configuration of the antennas, which is still the standard for GPR acquisitions. The results obtained at the test-site can be considered a first validation of the proposed procedure. The characteristics of the Liangzhu Site are nonetheless challenging and the present achievements are therefore a promising indicator of the potential performance of the method. The limitation to a 2-D experiment is certainly a major one and the extension to 3-D GPR is certainly crucial to map the prehistoric remains in terms of their actual extension and shape and to provide a classification of the targets of potential archaeological interest.

ACKNOWLEDGEMENTS

The first author of this paper undertook this work with the support of the 'ICTP TRIL Programme, Trieste, Italy'. The research work is further supported by the Major Program of the National Social Science Fund of China (No. 13&ZD192). Besides, the authors gratefully acknowledge the support of the Archaeological Institute of Zhejiang Province during data acquisition and archaeological interpretation. Moreover, we thank Antonios Vafidis and Nikos Spanoudakis of the Technical University of Crete, Greece for providing GPR-Pro Matlab tool. We also thank the Editor Prof. Mark E. Everett and another two anonymous reviewers for providing thoughtful and useful suggestions.

REFERENCES

Batey, R.A., 1987. Subsurface interface radar at Sepphoris, Israel, 1985, *J. Field Archaeol.,* **14,** 1–8.

Bevan, B. & Kenyon, J., 1975. Ground-penetrating radar for historical archaeology, *MASCA Newslett.,* **11**(2), 2–7.

Bini, M., Fornaciari, A., Ribolini, A., Bianchi, A., Sartini, S. & Coschino, F., 2010. Medieval phases of settlement at Benabbio castle, Apennine mountains, Italy: evidence from ground penetrating radar survey, *J. Archaeol. Sci.,* **37**(12), 3059–3067.

Böniger, U. & Tronicke, J., 2010. Integrated data analysis at an archaeological site: a case study using 3D GPR, magnetic, and high-resolution topographic data, *Geophysics,* **75**(4), B169–B176.

Booth, A., Linford, N.T., Clark, R.A. & Murray, A., 2008. Three-dimensional, multi-offset Ground-penetrating Radar imaging of archaeological targets, *Archaeol. Prospect.,* **15,** 93–112.

Booth, A.D., Clark, R.A., Hamilton, K. & Murray, T., 2010. Multi-offset ground penetrating radar methods to image buried foundations of a medieval town wall, Great Yarmouth, UK, *Archaeol. Prospect.,* **17**(2), 103–116.

Capizzi, P. & Cosentino, P.L., 2008. GPR multi-component data analysis, *Near Surface Geophys.,* **6**(2), 87–95.

Clarke, C.M., Utsi, E. & Utsi, V., 1999. Ground penetrating radar investigations at North Ballachulish Moss, Highland, Scotland, *Archaeol. Prospect.,* **6**(2), 107–121.

Conyers, L.B., 2004. Moisture and soil differences as related to the spatial accuracy of GPR amplitude maps at two archaeological test sites, in *Proceedings of the 10th International Conference on Ground Penetrating Radar,* Delft, The Netherlands, pp. 435–438.

Conyers, L.B., 2010. Ground-penetrating radar for anthropological research, *Antiquity,* **84,** 1–11.

Conyers, L.B., 2011. Discovery, mapping and interpretation of buried cultural resources non-invasively with ground-penetrating radar, *J. Geophys. Eng.,* **8,** S13–S22.

Conyers, L.B., 2012. *Interpreting Ground-Penetrating Radar for Archaeology,* Left Coast Press.

Conyers, L.B., 2013. *Ground-Penetrating Radar for Archaeology,* 3rd edn, AltaMira Press.

Conyers, L.B. & Goodman, D., 1997. *Ground-Penetrating Radar: An Introduction for Archaeologists,* AltaMira Press.

Conyers, L.B. & Leckebusch, J., 2010. Geophysical archaeology research agendas for the future: some ground-penetrating radar examples, *Archaeol. Prospect.,* **17,** 117–123.

Creasman, P.P., Sassen, D., Koepnick, S. & Doyle, N., 2010. Ground-penetrating radar survey at the pyramid complex of Senwosret III at Dahshur, Egypt, 2008: search for the lost boat of a Pharaoh, *J. Archaeol. Sci.,* **37**(3), 516–524.

Davis, J.L. & Annan, A.P., 1989. Ground-penetrating radar for high-resolution mapping of soil and rock stratigraphy, *Geophys. Prospect.,* **37,** 531–551.

Davis, J.L., Annan, A.P., Black, G. & Leggatt, C.D., 1985. Geological sounding with low frequency radar, in *Proceedings of the 55th Annual International Meeting of the Society of Exploration Geophysicists,* Extended Abstracts, Washington, DC, pp. 5–7.

Drahor, M.G., Berge, M.A. & Öztürk, C., 2011. Integrated geophysical surveys for the subsurface mapping of buried structures under and surrounding of the Agios Voukolos Church in Izmir, Turkey, *J. Archaeol. Sci.,* **38**(9), 2231–2242.

Everett, M.E., 2013. *Near-Surface Applied Geophysics,* Cambridge Univ. Press.

Fisher, E., McMechan, G.A. & Annan, A.P., 1992. Acquisition and processing of wide-aperture ground-penetrating radar data, *Geophysics,* **57,** 495–504.

Forte, E. & Pipan, M., 2008. Integrated seismic tomography and ground-penetrating radar (GPR) for the high-resolution study of burial mounds (tumuli), *J. Archaeol. Sci.,* **35,** 2614–2623.

Forte, E., Pipan, M. & Casabianca, D., DiCuia, R. & Riva, A., 2012. Imaging and characterization of a carbonate hydrocarbon reservoir analogue using GPR attributes, *J. Appl. Geophys.,* **81,** 76–87.

Francese, R.G., Finzi, E. & Morelli, G., 2009. 3-D high-resolution multichannel radar investigation of a Roman village in Northern Italy, *J. Appl. Geophys.,* **67,** 44–51.

Gaffney, C., 2008. Detecting trends in the prediction of the buried past: a review of geophysical techniques in archaeology, *Archaeometry,* **50**(2), 313–336.

Gaffney, V.L., Patterson, H., Piro, S., Goodman, D. & Nishimura, Y., 2004. Multimethodological approach to study and characterize Forum Novum (Vescovio, Italy), *Archaeol. Prospect.,* **11,** 201–212.

Goodman, D., Nishimura, Y. & Rogers, J.D., 1995. GPR time-slices in archaeological prospection, *Archaeol. Prospect.,* **2,** 85–89.

Goodman, D. & Piro, S., 2013. *GPR Remote Sensing in Archaeology,* Springer-Verlag.

Grasmueck, M., 1996. 3-D ground-penetrating radar applied to fracture imaging in gneiss, *Geophysics,* **61**(4), 1050–1064.

Grealy, M., 2006. Resolution of ground-penetrating radar reflections at differing frequencies, *Archaeol. Prospect.,* **13**(2), 142–146.

Jol, H.M., 1995. Ground penetrating radar antennae frequencies and transmitter powers compared for penetration depth, resolution and reflection continuity, *Geophys. Prospect.,* **43**(5), 693–709.

Kostadinova-Avramova, M. & Kovacheva, M., 2013. The magnetic properties of baked clays and their implications for past geomagnetic field intensity determinations, *Geophys. J. Int.,* **195**(3), 1534–1550.

Leckebusch, J., 2003. Ground-penetrating radar: a modern three-dimensional prospection method, *Archaeol. Prospect.,* **10,** 213–240.

Leucci, G. & Negri, S., 2006. Use of ground penetrating radar to map subsurface archaeological features in an urban area, *J. Archaeol. Sci.,* **33,** 502–512.

Linford, N., Linford, P., Martin, L. & Payne, A., 2010. Stepped frequency ground-penetrating radar survey with a multi-element array antenna: results from field application on archaeological sites, *Archaeol. Prospect.,* **17**(3), 187–198.

Liu, B., 2008. Excavations on the city-walls of the Liangzhu city-site in 2006 and 2007, *Cultural Relics,* **7,** 3–10 (in Chinese).

Lualdi, M. & Lombardi, F., 2014. Effects of antenna orientation on 3-D ground penetrating radar surveys: an archaeological perspective, *Geophys. J. Int.,* **196**(2), 818–827.

Morey, R.M., 1974. Continuous subsurface profiling by impulse radar, in *Proceedings of Engineering Foundations Conference on Subsurface Exploration for Underground Excavations and Heavy Construction,* Henniker, N.H., pp. 213–232.

Neubauer, W., Eder-Hinterleitner, A., Seren, S. & Melichar, P., 2002. Georadar in the Roman civil town Carnuntum, Austria: an approach for archaeological interpretation of GPR data, *Archaeol. Prospect.,* **9,** 135–156.

Nuzzo, L., Leucci, G., Negri, S., Carrozzo, M.T. & Quarta, T., 2002. Application of 3-D visualization techniques in the analysis of GPR data for archaeology, *Ann. Geophys.,* **45**(2), 321–337.

Oldfield, F. & Crowther, J., 2007. Establishing fire incidence in temperate soils using magnetic measurements, *Palaeogeog. Palaeclimat. Palaeoecol.,* **249**(3), 362–369.

Pipan, M., Baradello, L., Forte, E. & Prizzon, A., 2000. Polarization and Kinematic effects in Azimuthal investigations of linear structures with ground penetrating radar, in *Proceedings of the Symposium on the Application of Geophysics to Engineering and Environmental Problems,* Keystone, CO, pp. 407–413.

Pipan, M., Baradello, L., Forte, E. & Finetti, I., 2001. Ground penetrating radar study of iron age tombs in southeastern Kazakhstan, *Archaeol. Prospect.,* **8,** 141–155.

Radzevicius, S.J. & Daniels, J.J., 2000. Ground penetrating radar polarization and scattering from cylinders, *J. Appl. Geophys.,* **45**(2), 111–125.

Reynolds, J.M., 2011. *An Introduction to Applied and Environmental Geophysics,* 2nd edn, Wiley.

Roberts, R.L. & Daniels, J.J., 1996. Analysis of GPR polarization phenomena, *J. Environ. Eng. Geophys.,* **1**(2), 139–157.

Sassen, D.S. & Everett, M.E., 2009. 3-D polarimetric GPR coherency attributes and full waveform inversion of transmission data for characterizing fractured rock, *Geophysics,* **74**(3), J23–J34.

Shi, X., 1938. *Liangzhu: Preliminary Report on Pottery Cultural Site,* Education of Zhejiang Province Press (in Chinese).

Slob, E., Sato, M. & Olhoeft, G., 2010. Surface and borehole ground-penetrating-radar developments, *Geophysics,* **75**(5), 75A103–75A120.

Smith, D.G. & Jol, H.M., 1995. Ground penetrating radar: antenna frequencies and maximum probable depths of penetration in quaternary sediments, *J. Appl. Geophys.,* **33,** 93–100.

Taner, M.T., Schuelke, J.S., O'Doherty, R. & Baysal, E., 1994. Seismic attributes revisited, in *SEG Technical Program Expanded Abstracts,* pp. 1104–1106.

Tite, M.S. & Mullins, C., 1971. Enhancement of the magnetic susceptibility of soils on archaeological sites, *Archaeometry,* **13**(2), 209–219.

Trinks, I., Johansson, B., Gustafsson, J., Emilsson, J., Friborg, J., Gustafsson, C., Nissen, J. & Hinterleitner, A., 2010. Efficient, large-scale archaeological prospection using a true three-dimensional ground-penetrating radar array system, *Archaeol. Prospect.,* **17,** 175–186.

Trinks, I., Neubauer, W. & Hinterleitner, A., 2014. First high-resolution GPR and magnetic archaeological prospection at the viking age settlement of Birka in Sweden, *Archaeol. Prospect.,* **21,** 185–199.

Tsoflias, G.P., VanGestel, J.-P., Stoffa, P.L., Blankenship, D.D. & Sen, M., 2004. Vertical fracture detection by exploiting the polarization properties of ground-penetrating radar signals, *Geophysics,* **69,** 803–810.

Urban, T.M., Rowan, Y.M. & Kersel, M.M., 2014. Ground-penetrating radar investigations at Marj Rabba, a Chalcolithic site in the lower Galilee of Israel, *J. Archaeol. Sci.,* **46,** 96–106.

Vafidis, A. *et al.*, 2005. Integrated geophysical studies at ancient Itanos (Greece), *J. Archaeol. Sci.,* **32**(7), 1023–1036.

Viberg, A., Trinks, I. & Lidén, K., 2011. A review of the use of geophysical archaeological prospection in Sweden, *Archaeol. Prospect.,* **18**(1), 43–56.

Weaver, W., 2006. Ground-penetrating radar mapping in clay: success from South Carolina, USA, *Archaeol. Prospect.,* **13**(2), 147–150.

Yalçiner, C.Ç., Bano, M., Kadıoğlu, M., Karabacak, V., Meghraoui, M. & Altunel, E., 2009. New temple discovery at the archaeological site of Nysa (western Turkey) using GPR method, *J. Archaeol. Sci.,* **36**(8), 1680–1689.

Zhao, W., Forte, E., Pipan, M. & Tian, G., 2013a. Ground penetrating radar (GPR) attribute analysis for archaeological prospection, *J. Appl. Geophys.,* **97,** 107–117.

Zhao, W., Tian, G., Wang, B., Forte, E., Pipan, M., Lin, J., Shi, Z. & Li, X., 2013b. 2D and 3D imaging of a buried prehistoric canoe using GPR attributes: a case study, *Near Surface Geophys.,* **11**(4), 457–464.

Zhao, W., Forte, E., Levi, S.T., Pipan, M. & Tian, G., 2015. Improved high-resolution GPR imaging and characterization of prehistoric archaeological features by means of attribute analysis, *J. Archaeol. Sci.,* **54,** 77–85.

Zhao, Y., 2001. Excavation of the Mojiaoshan Site at Yuhang in 1992 and 1993, *Cultural Relics,* **12,** 4–19 (in Chinese).